A&A manuscript no.
(will be inserted by hand later)

Your thesaurus codes are:
08(02.12.2; 02.12.3; 08.02.1; 08.03.2; 08.09.2: HR 4049; 08.16.4)

ASTRONOMY
AND
ASTROPHYSICS
1.2.2008

The optical spectrum of HR 4049 * **

(includes a line identification from 3650 to 10850 Å)

Eric J. Bakker[1,2], Frank L.A. Van der Wolf[1,2], Henny J.G.L.M. Lamers[1,2], Austin F. Gulliver[3], Roger Ferlet[4], and Alfred Vidal-Madjar[4]

[1] Astronomical Institute, University of Utrecht, P.O.box 80000, NL-3508 TA Utrecht, The Netherlands
[2] SRON Space Research Laboratory, Sorbonnelaan 2, NL-3584 CA Utrecht, The Netherlands
[3] Department of Physics & Astronomy, Brandon University, Brandon, MB R7A 6A9, Canada
[4] Institut d'Astrophysique de Paris, CNR 98 bis Boulevard Arago, F-75014 Paris, France

received: February 1 1995, accepted: July 25 1995

Abstract. High-resolution optical spectra (UES/WHT) of the extreme metal-poor post-AGB star HR 4049 were obtained at four different orbital phases. The spectra cover the wavelength region from 3650 Å to 10850 Å at a resolution of $R = 5.2 \times 10^4$. These observations are supplemented with four high-resolution spectra of the NaI D1 & D2 and CaII K lines at $R \approx 10^5$ (CAT/CES). The optical spectrum shows 217 spectral lines: the Balmer series (Hα - H35), the Paschen series (P9 - P23), NI, OI and numerous CI lines. We show that the lines of Hα, Hβ, Hγ and NaI D show significant changes in profile between different observation dates. Nine components were identified in the profile of the NaI D lines of which three are circumstellar and six interstellar. The stronger CI lines are asymmetric and we derive a post-AGB mass-loss of $\dot{\rm M} = 6 \pm 4 \times 10^{-7}$ M$_\odot$ yr^{-1} from the asymmetry. The [OI] 6300 Å line has been detected in emission at the system velocity and we argue that the emission is from an almost edge-on disk with a radius of about 20 R_*.

Key words: line identification - line profiles - binaries: close - stars: chemical peculiar - stars: HR 4049 - stars: AGB and post-AGB

1. Introduction

HR 4049 (HD 89353) (see Table 1) is a member of the family of extremely metal poor post-AGB stars in a close binary system with a yet unseen companion star (Waelkens *et al.* 1991a, Van Winckel *et al.* 1994). The semi-major axis of the system of $a \sin i = 3R_*$ (Van Winckel *et al.* 1994) is smaller than the radius of HR 4049 during the preceding AGB phase ($\approx 200R_*$). This means that there was a common envelope evolution without spiraling in of the secondary. The time scale for circularization in a common envelope phase is very short. The fact that HR 4049 has an eccentricity of $e = 0.31$ suggest that binary interaction, possible with a circumsystem disk, are able to decircularize the orbit. With a semi-major axis of the binary smaller than the size of the star during the previous AGB phase it is not clear how this system could have survived the AGB.

The abundance pattern with iron a factor $10^{-4.8}$ under abundant and C, N, O and S close to solar, cannot be explained in terms of nucleo-synthesis products, but resembles that of the depleted interstellar gas. It is thought that the low abundance of the metals is due to a mechanism by which first the metals are condensed on dust in the circumstellar environment, followed by a separation of the dust and gas. The metal-poor gas then falls on the star and forms a photosphere of low metalicity, containing at least 10^{-5} M$_\odot$, which can only be sustained as long as there is no significant convection or strong stellar wind (Mathis & Lamers 1992; Waters *et al.* 1992). Taking a typical post-AGB mass-loss rate of $\dot{\rm M} \approx 10^{-7}$ to 10^{-8} M$_\odot$ yr^{-1}, the depleted photosphere would disperse in about a 100 years.

With this study we make a first attempt to study variations of the complete optical spectrum. The basis for this study is the line identification list presented in Table 11

Send offprint requests to: Eric J. Bakker, present address: Astronomy Department, University of Texas, Austin, TX 78712-1083, U.S.A., ebakker@astro.as.utexas.edu

* Based on observations obtained with the WHT/UES (La Palma) and CAT/CES (ESO)

** Fig. 9 and Table 11 are only available in electronic form at the CDS via anonymous ftp 130.79.128.5

(published at CDS), in which the profile parameters and the identification are given for all observed spectral features from 3650 Å to 10850 Å . The spectrum with the identifications is shown in Fig. 9 (at CDS).

Table 1. HR 4049 (HD 89353; SAO 178644)

		reference
m_v	+5.520	1
epoch	JD($\phi = 0.0$)=2447235 ± 3	1
period Π	429 ± 2 d.	2
$v_{\rm system}$	-32.9 ± 0.7 km s^{-1}	2
e	0.31	2
$a \sin i$	0.583 AU=3R_*	2
$f(m)$	0.143 M$_\odot$	2
$T_{\rm eff}$	7500 K	3
$\log g$	1.0 cm s^{-2}	3
M_*	0.54 M$_\odot$	4
R_*	38 R$_\odot$	4
L_*	4.1×10^3 L$_\odot$	

1: Waelkens *et al.* 1991a; 2: van Winckel *et al.* 1994; 3: Lambert *et al.* 1988; 4: Trams 1991

The observations and data reduction are discussed in Sect. 2. In Sect. 3 a description is given of the method of line identification and the criteria used for identification. The resulting list is given in Table 11 (at CDS) and Fig. 9 (at CDS). In Sect. 4 we discuss a number of selected lines: CI, NI and OI, Hydrogen lines, resonance lines of NaI and CaII and the [OI] at 6300 Å . In Sect. 5 the post-AGB mass-loss rate is derived from the asymmetry of the CI line profile and in Sect. 6 the conclusions of this work are summarized.

2. The observations and data reduction

2.1. WHT/UES observations

HR 4049 was observed from La Palma with the 4.2m William Herschel Telescope (WHT) and the Utrecht Echelle Spectrograph (UES). A description of the WHT/UES is given by Unger (1992). The first observation was made during commissioning time in February 1992. This observation gave rise to an observation campaign from February to June 1993 in service time. A log of the WHT/UES observations is given in Table 2 where phases are calculated using the orbital parameters of Table 1. All observations with the WHT/UES were obtained with echelle 31 (31.6 grooves per mm), except on February 11 1993 when we used echelle 79. The wavelength coverage of echelle 31 is roughly a factor 2.5 larger than that of echelle 79.

Three central wavelength settings were used: 4020 Å, 5260 Å and 7127 Å covering a wavelength range from 3650 Å to 10850 Å. The wavelength coverage of echelle 31 are 5350-10850 Å for $\lambda_c = 7129$ Å, 4380-6965 Å for $\lambda_c = 5261$ Å and $3590 - 4665$ Å for $\lambda_c = 4020$ Å. There is overlap of spectral orders in the blue, but not in the red ($\lambda \geq 7000$ Å). A complete spectrum could be obtained within no more than 40 minutes at a resolution of $R = 5.2 \times 10^4$ corresponding to 6 km s^{-1}. The spectra were calibrated using a Th-Ar lamp. The internal accuracy of the wavelength scale is about 6 mÅ. After extraction of the echellograms, the spectral data has an external accuracy of about 6 km s^{-1}. For $\lambda \geq 9500$ Å no wavelength calibration of the Th-Ar lamp was available at the time of reduction, which give rise to a small wavelength drift up to about 0.2 Å (≈ 6 km s^{-1}).

Some problems were encountered in flatfielding the UES spectra. Neutral density filters caused fringe patterns on the flatfields. These filters were applied to diminish the intensity of the Tungsten lamp, used for the flatfield images. The TEK1 CCD (1024×1024 pixels) produces a fringe pattern caused by its coating. This fringing starts to become important for $\lambda \geq 6000$ Å. From 6500 Å to 9000 Å the fringe amplitude is about 2 to 3 %. From 9000 Å to 10000 Å it becomes dramatically worse, going up to 10 and even 20 % (Tinbergen 1994). This fringing pattern occurs in both the target image and flatfield so that it can be removed.

We checked the wavelength resolution of the UES by looking at unresolved telluric absorption lines at 6880 Å and found for the rotation lines of telluric O_2 absorption a full-width-full-maximum of ≈ 6 km s^{-1}, which is equivalent to a resolution of $R = 5 \times 10^4$. Using the identification and wavelength in the solar spectrum atlas from Moore *et al.* (1966) of the O_2 telluric band we find a small shift of 0.1 ± 0.3 km s^{-1} with a standard deviation of $\sigma = 2.5$ km s^{-1}.

In this study we have concentrated on the the observations from March 8 1993. The observations in February and April 1993 gave identical identifications. Differences occured because *i)* different detectors were used; *ii)* different echelles were used giving rise to a slightly different wavelength coverage; *iii)* variations in the S/N ratio occured between different observations.

The binary motion of HR 4049 causes a velocity shift for photospheric and wind lines, but not for interstellar and circumstellar lines.

2.2. CAT/CES observations

HR 4049 was observed at four different dates at high-resolution and high signal-to-noise ratio with the 1.4m Coudé Auxiliary Telescope (CAT) at ESO. The CAT was equipped with a Coudé Echelle Spectrometer (CES) and a Reticon detector giving a spectral resolving power of $R = 10^5$ which corresponds to 3 km s^{-1}. The wavelength calibration is achieved by means of many emission lines of Th-Ar hollow cathode lamp, which yields and internal

Table 2. Log of the WHT/UES observations of HR 4049

	Feb. 25 92	Feb. 11 93	Mar. 8 93	Apr. 5 93
JD	2448678	2449030	2449055	2449083
ϕ	0.36	0.18	0.24	0.31
$\delta v_{\oplus}$	9.4 km s^{-1}	14.4 km s^{-1}	4.4 km s^{-1}	-7.7 km s^{-1}
echelle	31.6	79	31.6	31.6
CCD	EEV3	TEK1	EEV6	TEK1
flatfields	No	Yes	Yes	Yes
λ_c	run (code)	run (code)	run (code)	run (code)
7128.9 Å	41655(1.1)	72597(2.1)	74256(3.1)	75240(4.1)
	90 sec.	90 sec.	90 sec.	120 sec.
5260.9 Å	41656(1.2)	72594(2.2)	74262(3.2)	75238(4.2)
	90 sec.	120 sec.	90 sec.	120 sec.
4020.0 Å	41660(1.3)	72592(2.3)	74269(3.3)	75230(4.3)
	300 sec.	60 sec.	1500 sec.	120 sec.

$v_{\odot} = v_{\rm obs} + \delta v_{\oplus}$

accuracy better than 0.3 km s^{-1} and an external accuracy of about 1 km s^{-1} (Ferlet & Dennefeld 1984).

The CAT/CES spectra with a typical wavelength coverage of 30 Å were centered around the resonance NaI D1 & D2 and CaII K lines and have a factor two higher resolution than the WHT/UES. The spectra centered around the NaI lines have been divided by the spectrum of a bright template star in order to remove the numerous atmospheric H_2O lines in this spectral range. A log of the CAT/CES observations is given in Table 3.

Table 3. Log of the CAT/CES observations of HR 4049

Date	JD	$\delta v_{\oplus}$ [km/s]	Int. [s]	ϕ	remark
Jan. 11 86	2446442	20.8	3600	0.15	CaII K
Jan. 12 86	2446443	20.4	1800	0.15	NaI D
Nov. 20 86	2446755	22.9	2200	0.88	CaII K
Nov. 27 86	2446762	23.8	3000	0.90	NaI D
Feb. 23 87	2446850	6.2	1800	0.10	NaI D

3. The line identification

3.1. The method

The first step in the line identification process was checking those ions expected to be present in the photosphere of a metal poor supergiant with $T_{\rm eff} = 7500$ K. This showed that the main contribution of the absorption lines are from HI, CI, NI, OI and the resonance lines of NaI and CaII. The second step in the line identification process was the use of this line identification list as input to the interactive line identification programs IDPORC and LINEID. A description of these programs is given by Gulliver and Stadel (1990). In both steps the same selection criteria for identification were used.

In the first step the identification was made by hand using the multiplet table of Moore (1959). A multiplet was considered detected if the lines within one multiplet were observed with relative equivalent width in acceptable agreement with the intensity values as given in the multiplet tables. A constraint on the identification is that the Doppler velocities of lines within one multiplet should be the same. Most of the absorption lines were identified using these two criteria. The remaining features, mostly single lines, were identified by comparing the central absorption wavelengths with several finding lists.

This first step left a great number of unidentified weak lines. In the second step LINEID and IDPROC were used to check the already identified lines and to give possible identifications of the unidentified lines. The identification program uses an extensive spectral database. After running the program, the total number of unidentified lines was reduced by a factor 10! Most of the previously unidentified lines appeared to be due to CI multiplets, which were not described in the multiplet tables that were used in the first step.

The identification list of absorption lines of the optical spectrum of HR 4049 is given in Table 11 (at CDS) and overplotted in Fig. 9 (at CDS). The central wavelengths of the absorption lines were measured by fitting Gaussian profiles to the observed profiles. Other parameters like central depth (D), Full-Width-Half-Maximum ($FWHM$) and equivalent width (W_{λ}) were derived from these fits. In case of weak or asymmetric lines an eyeball fit

was made to determine the central wavelength and central depth. The equivalent width was measured by integrating over the whole line profile.

In fitting the lines with Gaussian profiles we implicitly assumed that the line broadening is mainly due to Doppler broadening. For CI, NI and OI lines this seems to be correct, but the method fails in the case of Hydrogen lines. The line wings are formed at different velocities with respect to the line cores, which makes the profiles asymmetric. In these cases the equivalent width has been calculated by integration over the whole line profile.

If an absorption feature was blended by other features, an estimate of the central wavelength and other parameters was made by fitting several Gaussian curves to the observed profile. A fit to a blended profiles is not always unique and the values of D, $FWHM$ and W_λ are less accurate than those for isolated lines.

Waelkens *et al.* (1991b) found several absorption lines in the spectrum of HD 52961 which they could not identify. The extreme metal poor star HD 52961 belongs to the same group of post-AGB stars as HR 4049. It is therefore interesting to note that the unidentified lines in HD 52961 are also present in the spectrum of HR 4049 and identified as CI. The equivalent widths of these lines in HR 4049 are roughly a factor three lower than in HD 52961 (Table 4).

Waelkens *et al.* (1991b) suggest molecular lines of CH^+ in the wavelength ranges of 4204-4238 Å and 4284-4318 Å. From the work by Bakker *et al.* (1995) we know that two other post-AGB stars, HD 44179 (Red Rectangle) and HD 213985, show the $A^1\Pi - X^1\Sigma^+$ (0,0) band of CH^+ at 4240 Åin emission and absorption respectively. There are at least ten other post-AGB stars which show C_2 and CN absorption by gas in the AGB remnant (Bakker *et al.* 1995). We checked this wavelength region carefully for the presence of possible molecular absorption or emission lines and could not find any. This non-detection of molecules might be important as it distinguishes HR 4049 form other post-AGB stars.

We confirm the detection of the HeI 4471 Å absorption lines (Waelkens *et al.* 1991b) and present the first detection of the forbidden [OI] line at 6300.311 Å (see Fig. 8). Lambert *et al.* (1988) referred to this line in HR 4049 but they were not able to detect it. The UES spectrum have a S/N-ratio ≈ 100 and clearly shows an emission line at the system velocity of HR 4049.

A normal B9 supergiant shows no NaI D1 & D2 lines and a very small CaII K photospheric lines. All three lines are dominant in the optical spectrum of HR 4049 and are thus from non-photospheric origin.

3.2. Line identifications list

Description of line identification list

The format of the Table 11 (at CDS) is listed below. The parameters of the atomic and ionic transitions are listed in column 1 through 4. They were all taken from the input database to the LINEID program as described in Gulliver and Stadel (1990).

1. $\lambda_{\rm lab}$ [Å]: the laboratory wavelength of the identified absorption line. An $*$ is given when the runnumber is not 3 (March 8 93).
2. multiplet: the element and multiplet number of the given absorption line.
3. χ [eV]: the lower level excitation energy of the transition. If an accurate value could not be found in the literature, the entry is left blank.
4. $\log gf$: the oscillator strength of the transition. If an accurate value could not be found in the literature, the entry is left blank.
5. $\lambda_{\rm obs}$ [Å]: the observed central wavelength of the absorption feature. The estimated accuracy is about 3 km s^{-1}, based on the S/N ratio and internal accuracy of the calibration method.
6. D [%]: the observed depth of the central absorption relative to the continuum. A line to zero intensity gives a depression of 100%. A mean error of 2% is adopted.
7. W_λ [mÅ]: the observed equivalent width. The estimated error on the equivalent width is 10%. If one of the wings of the profile could not be measured (due to blending or no wavelength coverage of the spectrum) this entry is left blank.
8. $FWHM$ [km s^{-1}]: Full-Width-Half-Maximum of the absorption feature. The accuracy is dependent on the S/N ratio and is estimated at 3 km s^{-1}.
9. v_{rad} [km s^{-1}]: radial heliocentric velocity for the identified absorption feature. The accuracy is 3 km s^{-1}.
10. run: the number of the spectra are give in Table 2. They refer to the number which was assigned to this spectrum during the observations.
11. Q: quality factor for the identification of the absorption feature. Lines marked with **3** are positively uniquely identified. A quality of **2** means that line is lightly blended. Quality **1** lines are severely polluted or very weak and can not be used for further studies.
12. remarks on the line identification. **a**: asymmetric line profile; **b**: line profile is blended; **f**: forbidden line; **IS**: interstellar; **CS**: circumstellar

The number of lines identified for the species present in the spectrum of HR 4049 are summarized in Table 5.

4. Selected line profiles

4.1. CI, NI and OI lines profiles

The majority (54 %) of absorption lines in the optical spectrum of HR 4049 are from neutral C, N and O. These lines were used to make an accurate determination of the stellar velocity. This assumes that the CI, NI and OI lines do not experience any emission as the Hydrogen lines do. To check whether this is a reasonable assumption we have selected four strong CI lines and plotted their lines pro-

Table 4. C I lines in the spectrum of HR 4049 compared with observations of Waelkens *et al.* (1991b) in HD 52961 (see text)

λ_{lab} [Å]	Mult.	HR 4049 $\lambda_{\rm obs}$ [Å]	HR 4049 W_λ [mÅ]	HD 52961 $\lambda_{\rm obs}$ [Å]	HD 52961 W_λ [mÅ]	$\lvert v_{dif}\rvert$ [km s^{-1}]
4212.342	18.12	4212.057	11	4212.487	35	30.6
4223.360	18.11	4222.934	16	4223.383	56	31.9
4466.476	18.07	4466.138	15	4466.616	47	32.1
4477.472	18.06	4477.149	15	4477.635	46	32.6
4478.588	18.06	4478.273	30	4478.840	96	38.0

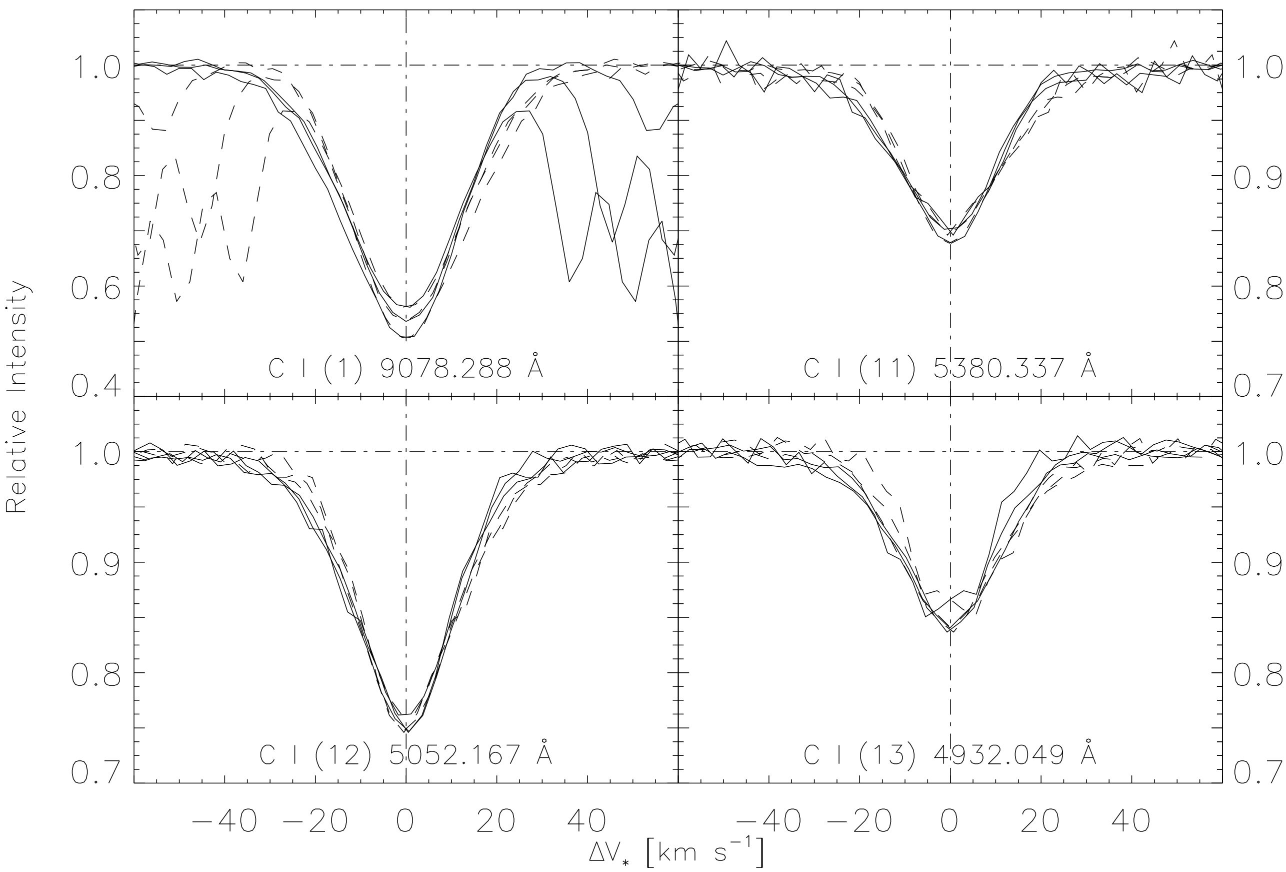

Fig. 1. Asymmetric CI lines. The dashed profiles represent the mirrored line profiles, to show the asymmetry. These mirrored profiles show that the absorption is stronger at the blue side of the profile at velocity $\Delta v_* \simeq -10$ to -40 km s^{-1}

files at three different phases during one orbital cycle (solid profiles in Fig. 1).

Only the CI line at $\lambda = 9078.288$ Å shows a change in strength whereas the other three CI lines do not show any change in strength. As the CI lines at $\lambda = 9078.288$ Å is in a part of the spectrum with numerous telluric lines, we attribute this change in intensity to a small error in the adopted continuum level. We conclude that the profiles did not vary in depth and equivalent width during the period we observed HR 4049.

To see whether the CI lines have a wind contribution we have mirrored the lines profiles on the average CI, NI and OI velocity (stellar velocity) and over plotted them (dashed profiles) with the observed lines profiles. We clearly see that in all twelve profiles the mirrored profile shows less absorption at negative velocities (-10 to

Table 5. Overview of observed spectral lines in the optical spectrum of HR 4049

ion	no. of lines	remark
H I	48	Hα - H35 and P9 -P23
HeI	1	4471 Å
C I	82	
N I	14	
O I	20	
[OI]	1	6300 Å
NaI	14	7 comp. in D
S I	9	
CaII	12	7 comp. in K & 3 in H & CaII(2)
unident	16	
Total	217	

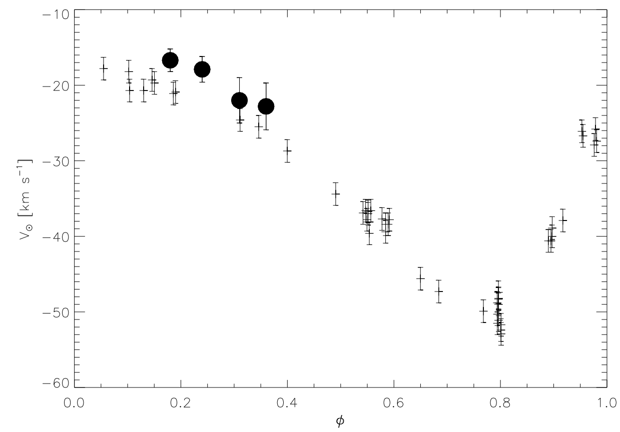

Fig. 2. Radial velocity curve for HR 4049. The filled circles represent data obtained in this study

-40 km s^{-1}) than the observed profile. In other words: the CI lines have stronger blue wings then red wings. This suggests a small contribution of the wind to the CI lines. We have also studied the N and O line profiles and found similar results. In order to exclude that the asymmetries are of instrumental origin, we have looked at the same lines in the spectrum of η Auri (A8Ia) and found that in this spectrum all (unblended) lines are symmetric. The symmetry is therefore not instrumental.

From Fig. 1 we conclude that the CI lines are a asymmetric, but the asymmetry does not seem to have changed during the period we observed HR 4049. It would be very interesting to study the asymmetry of the CI, NI and OI lines as function of orbital phase.

In Table 6 we have summarized the velocities of the CI, NI and OI lines. The asymmetry is too small to be of any importance for the determination of the stellar velocity from the CI, NI and OI lines. As expected there is no difference found between the average velocities of CI, NI and OI lines. The last column gives the adopted stellar velocity. Fig. 2 shows the stellar velocities versus orbital phase as determined from the work of Van Winckel *et al.* (1994). The new data points (solid dots) fit the overall radial velocity curve very well.

4.2. Hydrogen line profiles

The spectrum shows the Balmer lines from Hα to H35 and the Paschen lines from P9 to P23. There are very few stars known which can compete with HR 4049 in the number of Hydrogen lines observed in the spectrum. The part of the optical spectrum showing the Balmer (H8-H35) and Paschen (P11-P23) series is shown in Fig. 3. For a complete overview of the spectrum we refer to Fig. 9 available at CDS. Waelkens *et al.* (1991a) were the first to note that the shape of the Hα profile changes with orbital and photometric phase and attribute the Hα variability to changes in the wind structure caused by the presence of an unseen companion star.

In Fig. 4 we have plotted the four lowest Balmer lines on the dates we observed HR 4049. We see that not only the line profile of Hα, but also of Hβ and Hγ show changes with time. The first Balmer line which has only a photospheric contribution is Hϵ. From the figure we see that the cores of the Balmer lines are at the stellar velocity (corrected with the velocity of CI, NI and OI). Surprisingly this is even the case for the Hα lines. From Hα on April 1993 we find that the absorption is from gas with velocities between -50 and +50 km s^{-1} with respect to the star, suggesting that both infalling and outstreaming gas is observed at the same time. Using the stellar parameters (M_{*} and R_{*} in Table 1) we find $v_{escape} = 74$ km s^{-1}. Slightly larger than the observed outflow velocity of -50 km s^{-1}.

With such a complex wind geometry it is not trivial to estimate the mass-loss rate. We therefore tried to measure the Balmer progression in order to see whether material is accreting or that we are looking at wind material.

The upper three plots of Fig. 5 do not clearly show the presence of a Balmer progression. In February and March there seems to be a small negative progression, in April there seems to be a small positive progression. The Hα and Hβ lines (two highest $\log gf\lambda$ points) are filled in by emission. The lower three plots show the curve of growth (CoG) on three different dates. The observations of February 1992 were not included in Fig. 5 as this spectrum is from another orbital cycles and we know that the line profile variability does not repeat itself exactly from one cycle to another (Waelkens *et al.* 1991a). The three CoG show the optically thin part for $\log gf\lambda \leq -15.5$, the saturated part for $-15.5 \leq \log gf\lambda \leq -14.0$. For $\log gf\lambda \geq -14.0$ (Hα & Hβ) the emission component from the wind fills in the absorption and decreases the equivalent width. For the higher Balmer lines (small $\log gf\lambda$) the lines blend with

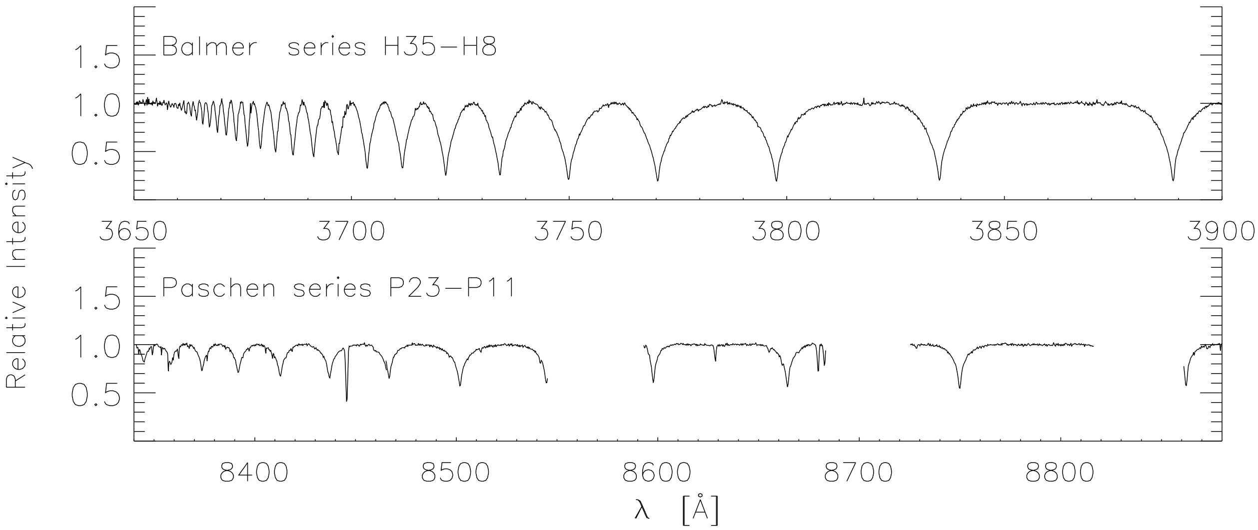

Fig. 3. The Balmer and Paschen series in the optical spectrum of HR 4049. The complete optical spectrum is given in Fig. 9 available at CDS

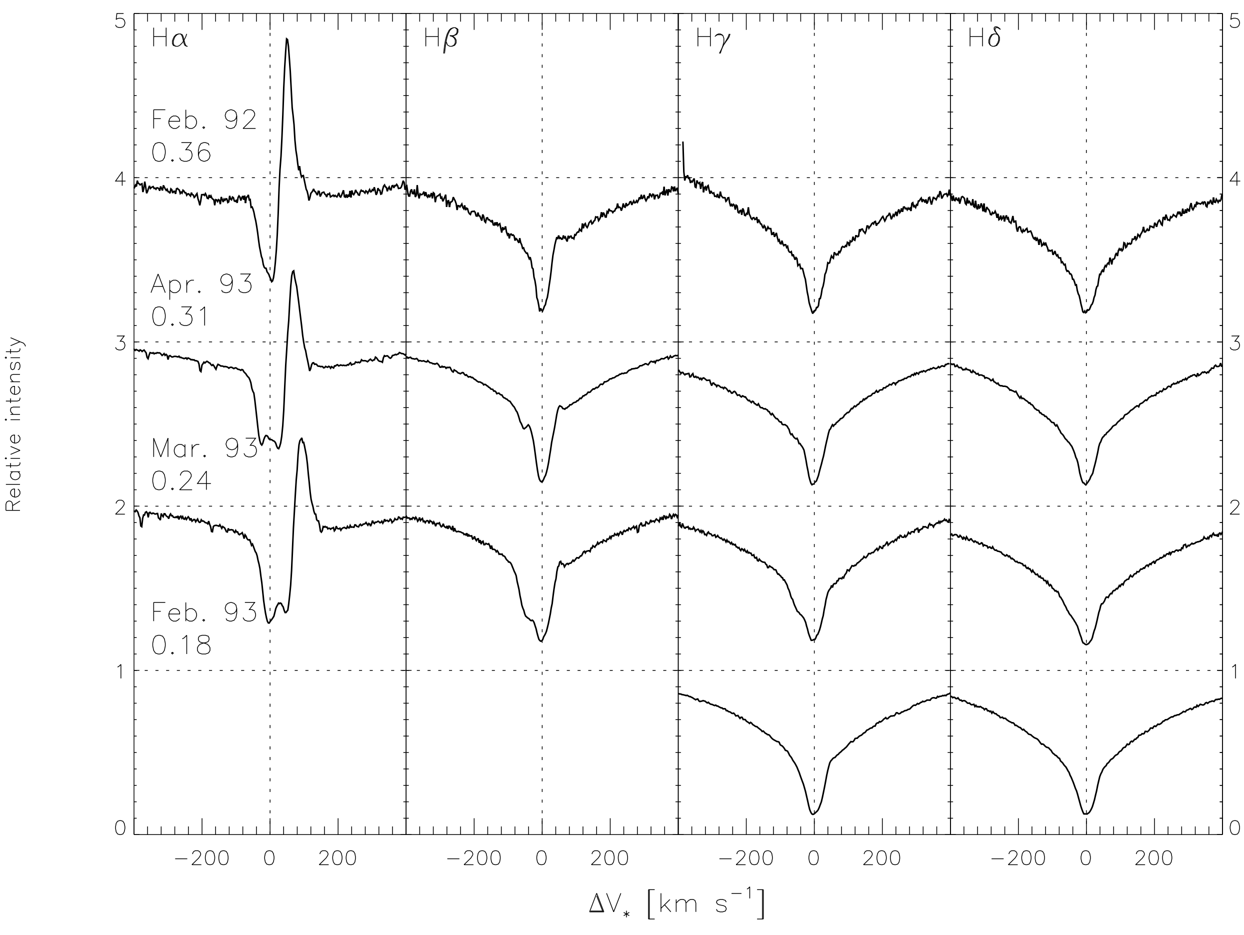

Fig. 4. The profiles of four Balmer lines at four different dates as function of velocity with respect to the stellar velocity. The spectra are plotted in order of orbital phase ($\phi = 0.18$, 0.24, 0.31, 0.36). Lines which are not plotted were not observed. Note that there is absorption on the red side of the stellar velocity in the Hα profile

Table 6. Radial velocities of the CI, NI and OI lines at different orbital phases with the standard deviation. Column 6 gives the averaged photospheric velocity based on the CI, NI and OI lines

Date	ϕ	C I	N I	O I	$v_{\mathrm{CI,NI,OI}}$
		[km s^{-1}]			
Febr. 12 1993	0.18	-16.1 ± 2.5	-15.3 ± 0.1[1]	-17.4 ± 2.4	-16.7 ± 2.5
Mar. 8 1993	0.24	-17.5 ± 1.9	-18.3 ± 2.0	-18.0 ± 1.1	-17.9 ± 1.7
Apr. 6 1993	0.31	-20.8 ± 2.6	-24.3 ± 3.8	-21.0 ± 2.6	-22.0 ± 3.0
Febr. 26 1992	0.36	-23.0 ± 4.0	-23.6 ± 2.7	-23.6 ± 3.1	-22.8 ± 4.7

[1] Only two lines of NI were observed on Febr. 12 1993

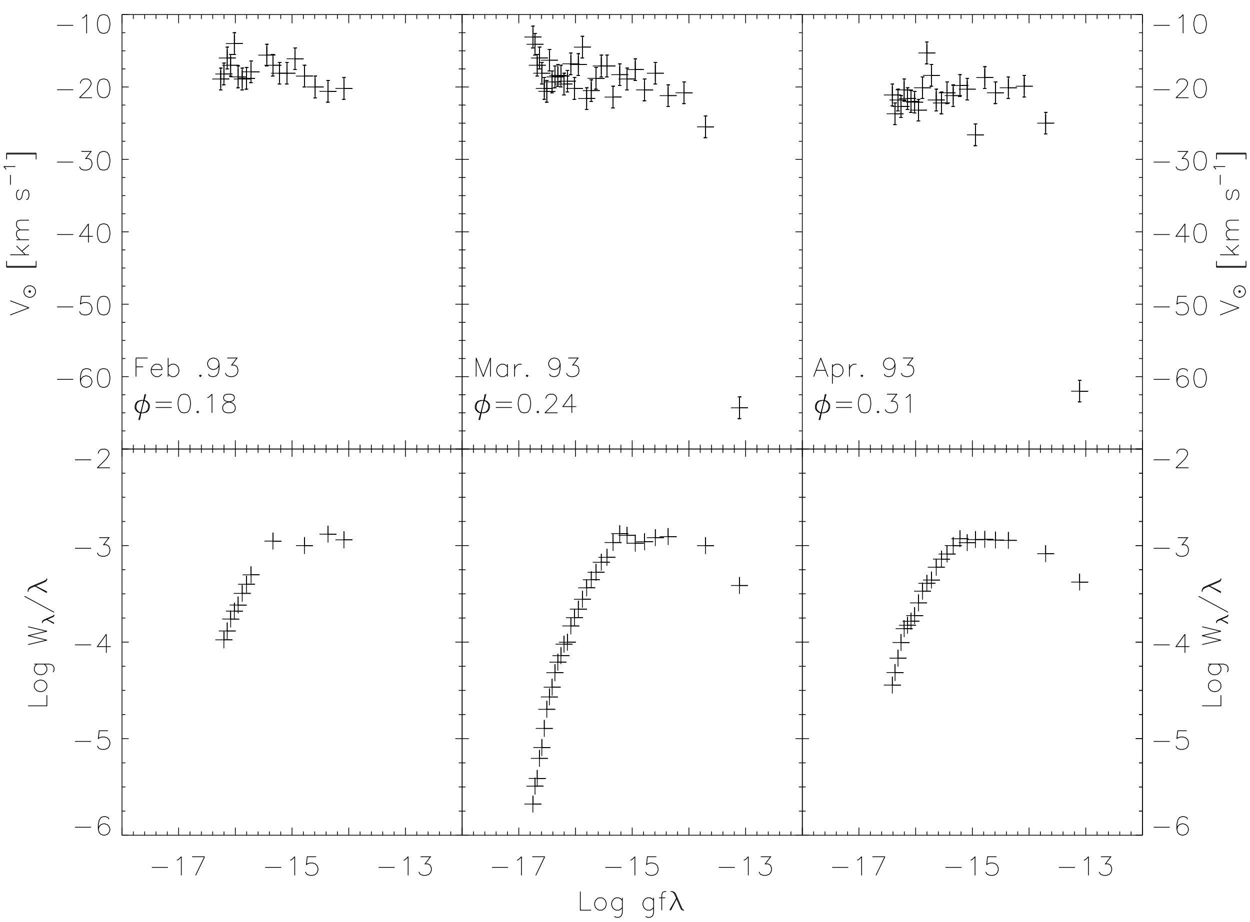

Fig. 5. The upper three plots show the Balmer progression at three different phases during one orbital cycle. The lower three plots show the curve of growth for the Hydrogen Balmer lines

each other and the continuum is no longer observed. This causes an underestimate of the equivalent width.

4.3. The resonance NaI D and CaII K lines

The strong resonance D lines of NaI and the H and K lines of CaII are the best tracers in the optical spectrum of the diffuse interstellar medium and circumstellar gas. From a study on the circumsystem extinction of HR 4049 by Waelkens *et al.* (1991a) we know that the circumsystem reddening changes with orbital phase. We looked for a relation between the strength of the component and the orbital phase. Such a relation could be important in understanding the extreme low metalicity of the photosphere of HR 4049 and could give an answer whether gas is still accreting. The left panel of Fig. 6 shows the NaI D1 & D2 lines and the CaII K line obtained with WHT/UES and

Fig. 7 shows one of the CAT/CES spectra of the NaI D1 & D2 lines. These spectra show clearly the presence of five different velocity components. To simplify the discussion we have coded the main absorption components in order of increasing wavelength as A, B, C, D and E. Component A, C and E are blends of smaller absorption lines.

To determine whether the NaI D1 & D2 and CaII H & K lines have a photospheric, wind, circumstellar and an interstellar contribution to the line profile, we will study the time variability of the absorption components. In Table 7 the central heliocentric velocities of all components have been listed in order of velocities. Five strong (A...E) absorption components could be identified of which three showed the presence of smaller absorption components. In total we found nine components. Table 7 shows that none of these absorption components shows radial velocity variation as function of orbital phase. This means that there is no, or a negligible photospheric contribution to the line profile and the line forming region is stationary with respect to the system velocity of HR 4049: inter- or circumstellar.

The first and the last spectrum are obtained 7.25 years apart which shows that no long term variations are observed. Components C, D and E have positive velocities with respect to the system velocity of -32.9 km s^{-1} suggesting that they are of interstellar origin. Component A2 is on the system velocity and it is therefore interesting to study the possibility that this line is formed in the circumsystem disk. Component A1 is at negative velocities with respect to the system velocity and could be due to the stellar wind at a terminal velocity of 15 km s^{-1}, much smaller than the outflow velocity derived from the Hα profile or the escape velocity. It is important to note that two of the spectra (CAS/CES) which have been obtained at the same orbital phase but from two successive cycles show an emission component which fills in the A absorption component. In one spectrum the emission component is even above the continuum level at $v_\odot = -44$ km s^{-1}. Such a strong change in line strength can only occur if the line forming region is close to the star. If we look at Fig. 2 we note that the emission in the NaI D lines occurs at apastron (radial velocity changes smoothly), thus when the observed star is closest to the circumsystem disk. We therefore interpret the emission as due to excitation of the circumsystem disk by the radiation field of the star.

In Table 8 the ratio of the observed equivalent width for each component is given relative to the equivalent width as measured on March 1993. The estimate of the error on the equivalent width is less than 10 %, but as different instrument are used and the equivalent width are measured by different persons using different techniques we will take a pessimistic estimate of the error of 25 %, meaning that all entries in Table 8 with values ≤ 0.7 or ≥ 1.2 indicate that the equivalent width has significantly changed. Component E has not been listed because the equivalent width is polluted by a telluric H_2O lines, component C and D are treated as one absorption component as they are severely blended with each other.

Table 8. Equivalent width of absorption components in NaI D1 & D2 and CaII H & K resonance lines relative to the March 1993 ($\phi = 0.24$) observation

ϕ	instr	line	A CS	B CS	C+D IS	remark
0.10	CAT	D1	0.7	0.4	0.8	
0.15	CAT	D1	0.8	0.4	0.8	
0.24	UES	D1	1.0	1.0	1.0	$\equiv 1.0$
0.31	UES	D1	1.0	0.7	1.0	
0.90	CAT	D1	3.0	0.3	0.9	
0.10	CAT	D2	0.8	0.5	0.9	
0.15	CAT	D2	0.8	0.5	0.9	
0.24	UES	D2	1.0	1.0	1.0	$\equiv 1.0$
0.31	UES	D2	1.0	0.7	1.0	
0.90	CAT	D2	2.4	0.2	0.8	
			A-D			
0.11	CAT	K	0.8			
0.15	CAT	K	1.0			
0.18	UES	K	1.2			
0.24	UES	K	1.0			$\equiv 1.0$
0.31	UES	K	1.1			
0.88	CAT	K	0.9			

This table shows that the C+D component shows no variations in the equivalent width over the orbital phase, but the A and B component do vary by a factor three in equivalent width! An extreme situation occurs for NaI D1 at $\phi = 0.90$ where the A component has increased in equivalent width by a factor three while the equivalent width of component B has decreased by a factor three. There is also a remarkable difference between the CAT/CES and UES/WHT spectra: in the first the component A is stronger than B, where in the second B is stronger than A (compare Fig. 6 and 7). However this data set is not suitable for a study on the exact dependence of the equivalent width on orbital phase, but is shows that the A and B component of NaI D1 & D2 lines are variable and are therefore not of interstellar origin.

Table 8 also shows the ratio of equivalent width of the CaII K lines at different dates with the equivalent width as measured on March 1993. No significant variations are found.

We have seen that components A (A1 & A2) and B change with time (and probably orbital phase). It is interesting to see whether the uniform data set of UES/WHT spectra show short time variation ($0.18 \leq \phi \leq 0.31$) at less than 25 %. The right panel of Fig. 6 shows the standard deviation (σ) on the spectra as function of velocity expressed in % to continuum level. The pollution by tel-

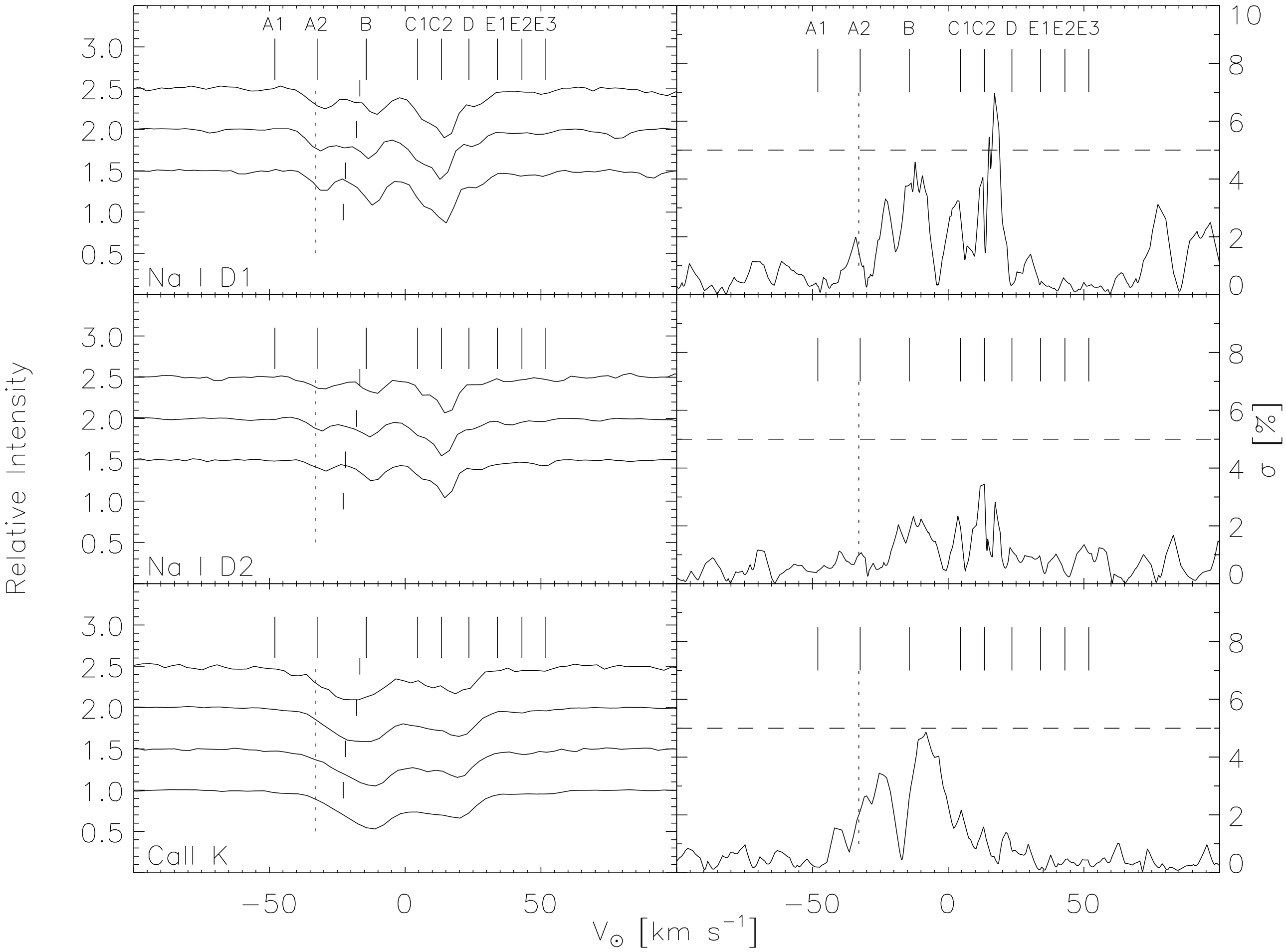

Fig. 6. Left: the resonance NaI D1 (top) & D2 (middle) and CaII K (bottom) lines are plotted on the velocity scale (from bottom to top: Febr. 93, Mar. 93, Apr. 93 and Feb. 92). The dashed line at -33 km s^{-1} is the system velocity and the stellar velocity is marked by a small dash at the continuum level. Right: the standard deviation of the four spectra as function of radial velocity expressed in percentage of the continuum level

luric water vapor shows up in the Na I D1 profile as sharp variations of less than 4 %. The NaI D2 is less polluted and does not show significant variations. The CaII K has smoothly changed for $v_\odot \leq 0$ km s^{-1}, but at a very low level.

We conclude that the components at C, D and E are probably of *interstellar* origin and the variable components A and B are of circumstellar origin. Component A might be from wind material with an outflow velocity of only 15.1 km s^{-1}. So far we have assumed that the A2 and B components are separate absorptions, but it is also possible that A2/B is one strong absorption with a central emission component. Such a situation can occur in a case of mass transfer in a binary system.

4.4. [OI] emission line

The presence of the [OI] line (χ = 0.0 eV) is of interest for the study of the circumstellar environment of HR 4049 as it is generally thought that forbidden lines are formed in low density gas. We therefore have looked in detail at the spectra for the presence of [OI] at 6300 Å. Although very weak, we argue that we have detected the [OI] at 6300 Å in emission at three different dates.

In Fig. 8 we have plotted the observed spectrum around 6300 Å at three different phases of one cycle. We did not correct for the earth motion, nor for the solar motion to show clearly the presence of [OI] in emission. The two “strong” absorption lines are telluric H_2O, while the emission lines at 6300.3 Å is the [OI] 6300.311 Å telluric line. These lines do not vary in position. A careful examination of this part of the spectrum shows that the emission around 6299.6 Å varies in position. This excluded the line from being telluric. Table 9 give the heliocentric corrected velocity of the [OI] lines for the three different dates.

The [OI] emission lines does not follow the orbital motion of the the CI, NI and OI lines, which excludes it from being photospheric. If we compare the [OI] ve-

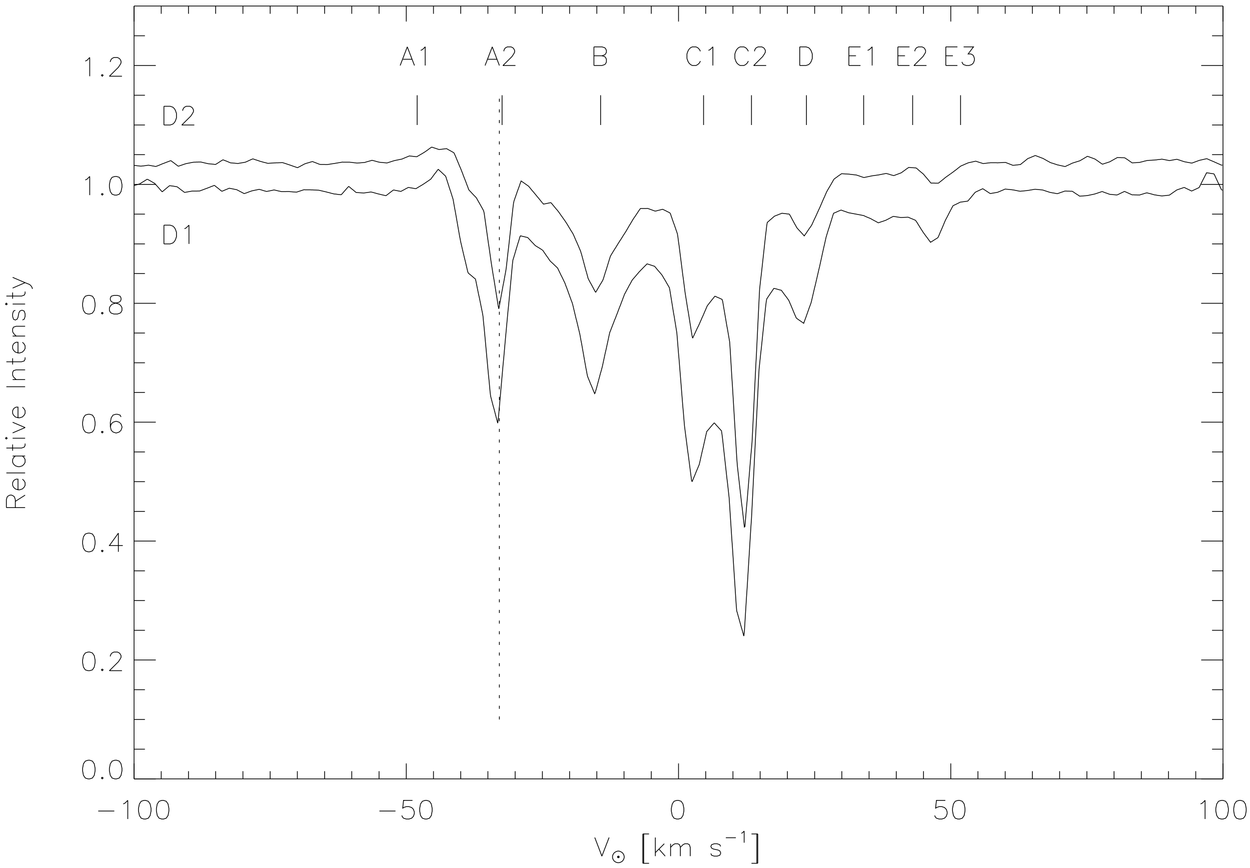

Fig. 7. NaI D1 & D2 lines observed on Jan. 12 1986 with CAT/CES when the star is closest to the circumsystem disk. This plot clearly shows the presence of an emission component at the blue edge of the NaI D1 & D2 profiles (near A1). The emission component is not present in the UES/WHT spectra

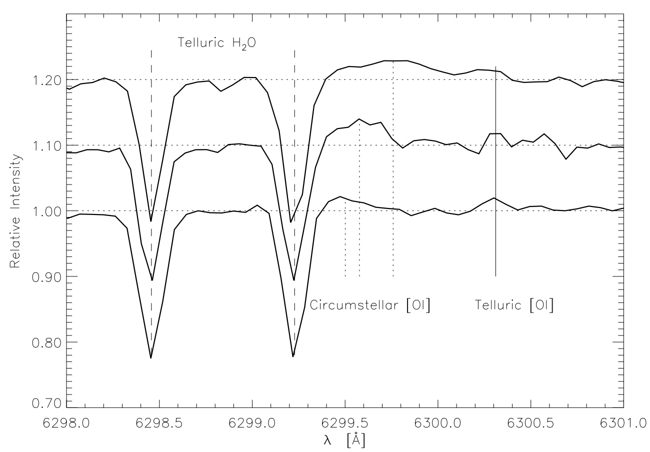

Fig. 8. [OI]F in 3 different WHT/UES spectra of HR 4049 (from bottom to top: Feb93, Mar93 and Apr93)

Table 9. Radial velocities (heliocentric) of the observed [OI] emission line at 6300 Å at different orbital phases. The system velocity is -32.9 km s^{-1}

Date	ϕ	v_{rad} [km s^{-1}]
Feb. 12 1993	0.18	-25.6
Mar. 8 1993	0.24	-31.0
Apr. 6 1993	0.31	-32.5
Average		-30 ± 2

locity of -30 ± 2 km s^{-1} with the system velocity of -32.9 ± 1.0 km s^{-1} found from an analysis of the orbital motion of the star (Van Winckel *et al.* 1994) we see that the [OI] emission is at the system velocity. From the March 1993 spectrum (with the highest signal-to-noise-ratio) we find a full-width-full-maximum of 20 km s^{-1}, but the ex-

Table 7. Velocities of absorption components in NaI D1 & D2 and CaII H & K resonance lines

ϕ	Instr	line	A1 CS	A2 CS	B CS	C1 IS	C2 IS	D IS	E1 IS	E2 IS	E3 IS
0.10	CAT	D1[1]		-34	-15	3	12	23			
0.15	CAT	D1[2]		-33	-15	4	12	23	37	47	
0.24	UES	D1		-29	-12	6	15	27			51
0.31	UES	D1		-32	-14	4	14	26		40	50
0.90	CAT	D1	-49	-34	-15	3	11	22		46	52
0.10	CAT	D2[1]		-33	-15	3	12	23			
0.15	CAT	D2[1]		-34	-15	4	11	22	37	46	
0.24	UES	D2		-30	-12	6	15	26		41	50
0.31	UES	D2		-31	-13	5	14	25			50
0.90	CAT	D2	-54	-35	-16	3	11	23	37	42	
0.15	CAT	K			-16	4	15		37	48	
0.18	UES	K	-45	-30	-14	5	15	22	32	43	53
0.24	UES	K		-33	-13	8	19		30	43	56
0.31	UES	K	-42	-29	-16	7	18	24		40	52
0.88	CAT	K		-39	-14	3	15				
0.24	UES	H[3]			-14		17				53
$\overline{v_\odot}$ [km s^{-1}]			-48 ± 3	-32.5 ± 0.7	-14.3 ± 0.3	4.5 ± 0.4	14.1 ± 0.6	23.8 ± 0.8	35 ± 1	43 ± 1	51.9 ± 0.7
$\delta v_{\rm system}$ [km s^{-1}]			-15	0.4	18.6	37.4	47.0	56.7	68	76	85

1: A1/A2 filled in by emission; 2: emission at -44 km s^{-1}; 3: blended with Hϵ

pansion velocity derived from the Hα profile is of the order of 50 km s^{-1} whereas the escape velocity is 75 km s^{-1}. [OI] should have a $FWFM$ of 100 km s^{-1} if it is formed in the stellar wind. As we only observe a $FWFM$ of 20 km s^{-1} the [OI] it is not formed in the stellar wind.

Lambert *et al.* (1988) found the CO first overtone in absorption at a velocity of -33.1 ± 0.2 km s^{-1} with a $T_{\rm excitation} = 300 \pm 100$ K. This CO cannot be of photospheric origin because the $T_{\rm exc}$ is too low, nor can it be formed in the wind as it is observed at the system velocity. Both the detection of [OI] and CO first overtone can be explained by the model of HR 4049 proposed by Waelkens *et al.* (1995) in which a circumsystem disk revolves around the binary. Assuming a Keplerian orbit of the circumsystem disk around HR 4049 with $v \sin i = 10$ km s^{-1} and taking the most likely $\sin i = \frac{1}{2}\sqrt{2}$ with the stellar param-

eters (Table 1) we find a distance of the [OI] disk of only $r_{[OI]} = 13R_*$.

The distance from the circumsystem disk to HR 4049 can be estimated in another way by fitting the near-IR excess to an optically thin dust model. This yields a dust inner radius of $r_{\rm inner} = 28R_*$ (Lamers *et al.* 1986), of the same order as the radius found from the [OI] emission line. Taking the dust inner radius and a Keplerian orbit yields a velocity of 10 km s^{-1} of the disk material. To fit the [OI] velocity to the dust inner radius the system has to be nearly edge-on ($i = 90^o$). This explains the detection of CO first overtone in absorption at the system velocity (in the disk) and the strong varying CS absorption (Waelkens *et al.* 1991a).

One of the puzzling questions of HR 4049 and related objects is the mass and spectral type of the unseen companion star. Taking $i = 90^o$ and the stellar parameters from Table 1 we find a mass of the companion star of 0.56 M$_\odot$: a White Dwarf or a low-mass main sequence star.

5. Discussion

5.1. Mass-loss rate from asymmetric CI lines

The asymmetry in the CI of Fig. 1 gives us a tool to determine the mass-loss rate. From the four profiles presented we will not use $\lambda = 9078$ Å because the continuum level is not accurate enough. For the lines at $\lambda = 5380$, 5052 and 4932 Å we find that the extra absorption on the blue wing has an equivalent width of respectively 9, 11 and 6 mÅ with and estimated error of 3 mÅ. Taking the $\log gf$ value from Table 11 and a statistical weight of $g_i = 3$ for all three transitions we find column densities of respectively 7.4×10^{12}, 6.5×10^{12} and 5.8×10^{12} cm^{-2}. All three transition are from the same lower level ($\chi = 7.68$ eV) which allows averaging of the column densities to $6.6 \pm 2.0 \times 10^{12}$ cm^{-2}. We did not observed any CII lines and neglected the CII contribution to the carbon abundance. The wind temperature is in the range $0.5T_{\rm eff} \leq T_{\rm wind} \leq 0.8T_{\rm eff}$ with $T_{\rm eff} = 7500$ K and we will adopt the upper limit of $0.8T_{\rm eff} = 6000$ K meaning that we determine a minimum mass-loss rate. Taking the analytic approximation of the partition function of CI from Gray (1992) of $U(T_{\rm wind}) = 0.975$ while assuming LTE we find a total column density for carbon of $N_C = 1.8{\pm}0.3{\times}10^{19}$ cm^{-2} and $N_H = 8.5{\pm}0.2{\times}10^{22}$ cm^{-2} taking the carbon abundance of HR 4049 from Lambert *et al.* (1988) of [C/H]=-0.2.

In order to determine the mass-loss $\dot{\rm M}$ we have to make an assumption about the depth of the line forming region. The terminal velocity is not well known from Hα because of the complex profile and we use the relation of a late B-type supergiant of $v_\infty = 1.1v_{\rm escape}$ found by Lamers *et al.* (1995). Taking the stellar parameters from Table 1 we find an escape velocity of $v_{\rm escape} = 75$ km s^{-1} and a terminal velocity of the wind of $v_\infty = 83$ km s^{-1}. In Sect. 4.1 we have shown that the wind component of the CI line profiles occurs at outflow velocities between $v_1 = 10$ km s^{-1} and $v_2 = 40$ km s^{-1}. With the velocity law adopted (Eq. 1) and a given β (Table 10) this gives the geometrical distance of the line forming region to the star. For $\beta = 0.5$ we find that the wind component is formed between $R_1 = 1.01R_*$ and $R_2 = 1.30R_*$.

$$V(r) = V_\infty \left(1 - \frac{R_*}{r}\right)^\beta \ [\mathrm{km\ s^{-1}}] \qquad (1)$$

Table 10. Mass-loss rates derived from the asymmetry of CI lines

β	r_1 [R_*]	r_2 [R_*]	$\dot{\rm M}$ ($T_{\rm wind} = 6000$ K) [$M_\odot$ yr^{-1}]
0.5	1.01	1.30	$9 \pm 3 \times 10^{-7}$
1.0	1.13	1.93	$4 \pm 3 \times 10^{-7}$
2.0	1.53	3.27	$4 \pm 3 \times 10^{-7}$

The lower limit on the mass-loss rates found (Table 10) is several times 10^{-7} M$_\odot$ yr^{-1} and from this we adopt a post-AGB mass-loss rate of HR 4049 of $\dot{\rm M} = 6 \pm 4 \times 10^{-7}$ M$_\odot$ yr^{-1}. This is the first time that the post-AGB mass-loss rate has been determined for HR 4049 and it shows that HR 4049 has a significant stellar wind. Monitoring the CI, NI and OI lines profiles over the orbital phase could give an answer about the mass-loss rate as a function of orbital phase.

6. Conclusion

With this paper we present a line identification list of the optical spectrum of HR 4049 from 3650 Å to 10850 Å . We have identified 48 lines from HI and 116 lines from neutral CI, NI and OI, confirm the detection of HeI at 4471 Å and present the first detection of [OI] 6300 Å emission at the system velocity.

Variability of the lines profiles is observed in Hα, Hβ and Hγ, but surprisingly also in the A & B components of the resonance NaI D1 & D2 lines and the CaII K line. At different orbital phases the line-of-sight traces different circumstellar material and results in a change of lines profile. The emission in the NaI D lines is interpreted as due to excitation of disk material by the radiation field of the star during apastron (the star is closest to the CS disk). Evidence for this model can be obtained by simultaneously observing the NaI D lines, Hα and the UV (circumstellar reddening).

The discussion on the CI, NI and OI lines profiles shows that the stronger C lines are asymmetric. The asymmetry can be explained as due to a stellar wind with a

mass-loss rate of $\dot{\mathrm{M}} = 6 \pm 4 \times 10^{-7}$ $\mathrm{M}_\odot$ yr^{-1}. This is the first time that the post-AGB mass-loss rate of HR 4049 has been determined.

The detection of [OI] in emission at the system velocity with a Full-Width-Full-Maximum of only 20 km s^{-1} is interpreted as due to an edge-on disk. For an edge-on system we find from the orbital parameters that the secondary has a mass of 0.56 $\mathrm{M}_\odot$. This can be a White Dwarf or a low-mass main sequence star.

Acknowledgements. The authors are very grateful to Rens Waters, Christoffel Waelkens, Norman Trams and René Oudmaijer for the stimulating and constructive discussions on this work. Ton Schoenmaker is acknowledged for his valuable contribution in reducing the UES spectra. EJB was supported by grant no. 782-371-040 by ASTRON, which receives funds from the Netherlands Organization for the Advancement of Pure Research (ZWO). This research has made use of the SIMBAD database, operated at CDS, Strasbourg, France.

References

Bakker E.J., Waters L.B.F.M., Lamers H.J.G.L.M., Schoenmaker T.: 1995, in: "Circumstellar Matter", Eds: G.D. Watt, P.M. Williams, p335-338

Ferlet R., Dennefeld M.: 1984, A&A 138, 303

Gray D.F.: 1992, "The observation and analysis of stellar photosphere", second edition

Gulliver A.F., Stadel J.G.: 1990, PASP 102, 598

Lambert D.L., Hinkle K.H., Luck R.E.: 1988, ApJ 333, 917

Lamers H.J.G.L.M., Waters L.B.F.M., Garmany C.D., Perez M.R., Waelkens C.: 1986, A&A 154, L20

Lamers H.J.G.L.M., Snow T.P., Lindholm D.: 1995, ApJ in press

Mathis J.S., Lamers H.J.G.L.M.: 1992, A&A 259, L239

Moore Ch.E., "A multiplet table of astrophysical interest: 1959, National Bureau of Standards", technical note 36

Moore Ch.E., Minnaert M.G.J., Houtgast J., "The solar spectrum 2395 Å to 8770 Å": 1966, National Bureau of Standards, Monograph 61

Tinbergen J.: 1994, Spectrum 1, 26

Trams N.R.: 1991, Ph.D. thesis, University of Utrecht, Netherlands

Unger S.: "UES user manual", 1992, May 12

Van Winckel H, Waelkens C., Waters L.B.F.M.: 1995, A&A 293, L25

Waelkens C, Waters L.B.F.M., Van Winckel H, Deams K.: 1995, in: "Circumstellar Matter", Eds: G.D. Watt, P.M. Williams, p357-360

Waelkens C., Lamers H.J.G.L.M., Waters L.B.F.M., Rufner F., Trams N.R., Le Bertre T., Ferlet R., Vidal-Madjar A.: 1991a, A&A 242, 433

Waelkens C., Van Winckel H., Bogaert E., Trams N.R.: 1991b, A&A 251, 495

Waters L.B.F.M., Trams N.R., Waelkens C.: 1992, A&A 262, L37

This article was processed by the author using Springer-Verlag LaTeX A&A style file *L-AA* version 3.

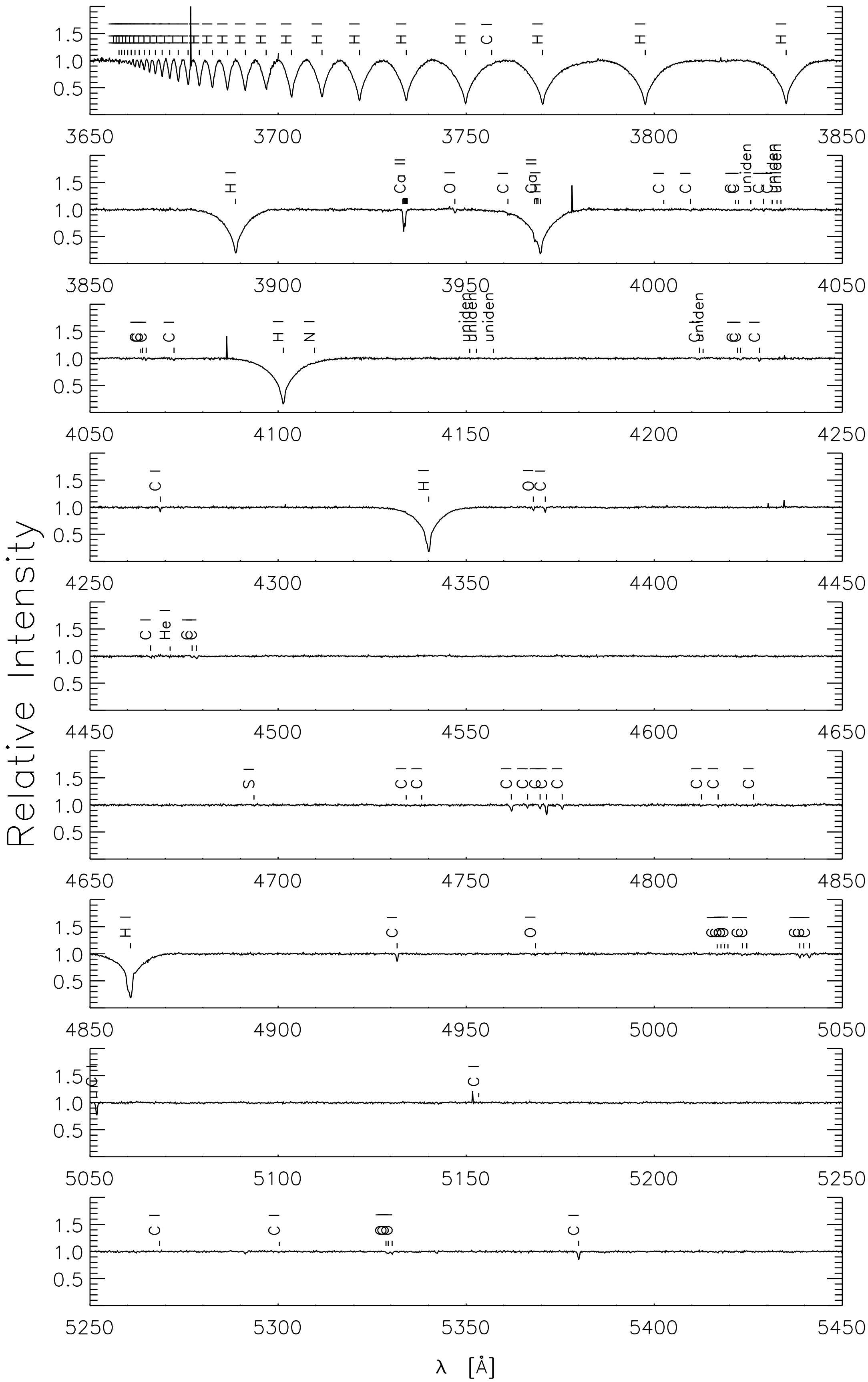

Fig. 9. The optical spectrum of HR 4049 from 3650 Å to 10850 Å

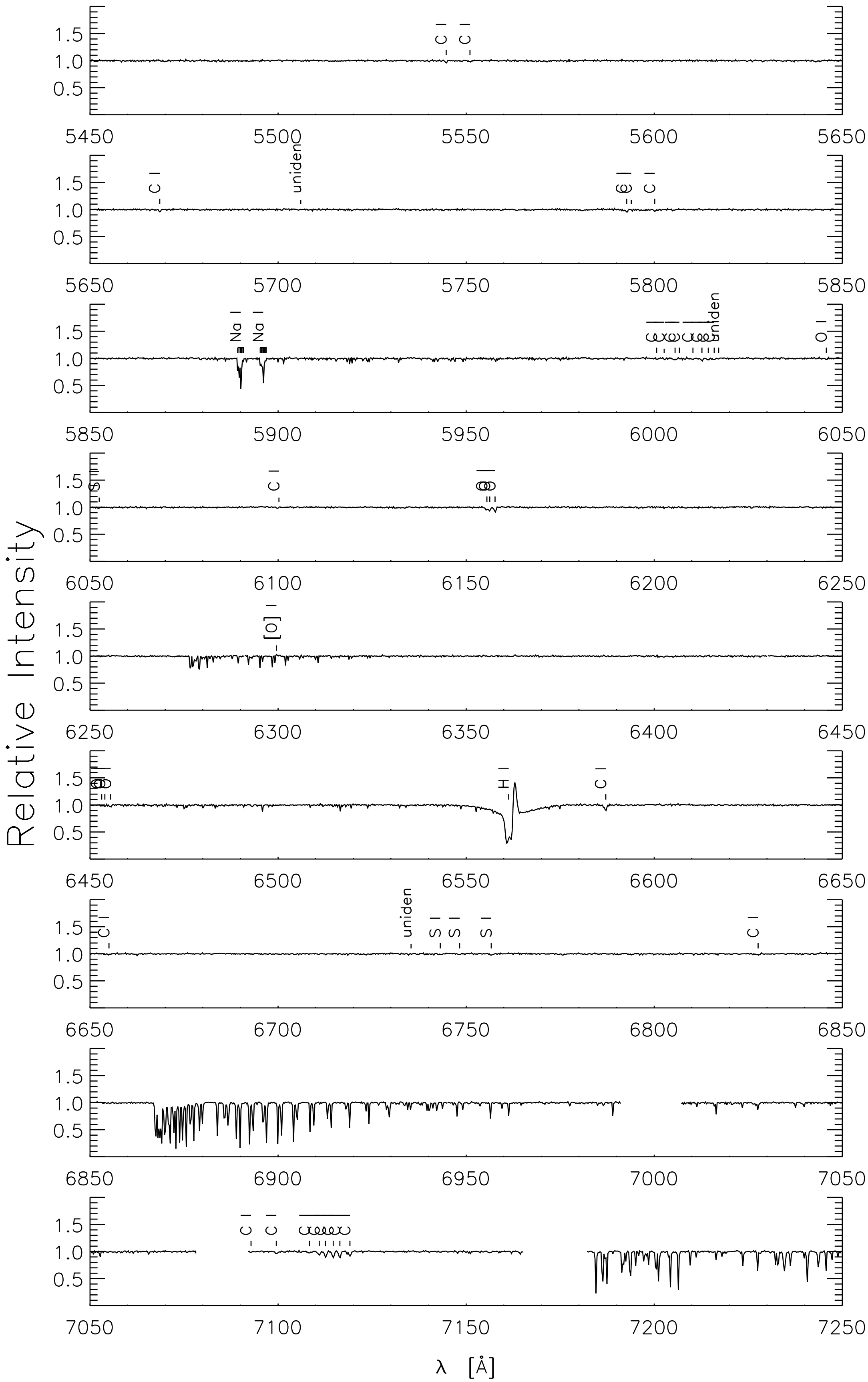

Fig. 9. continued

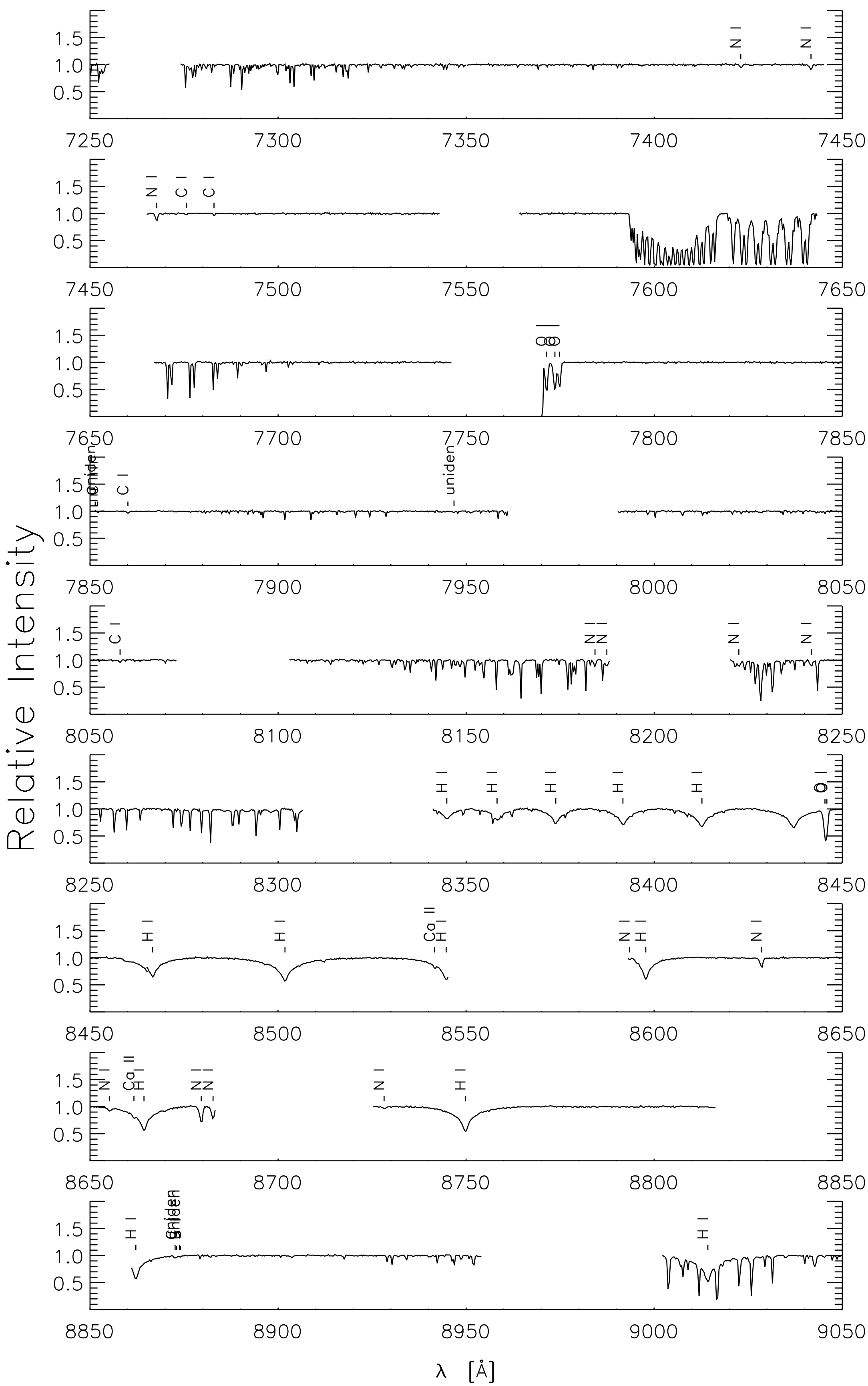

Fig. 9. continued

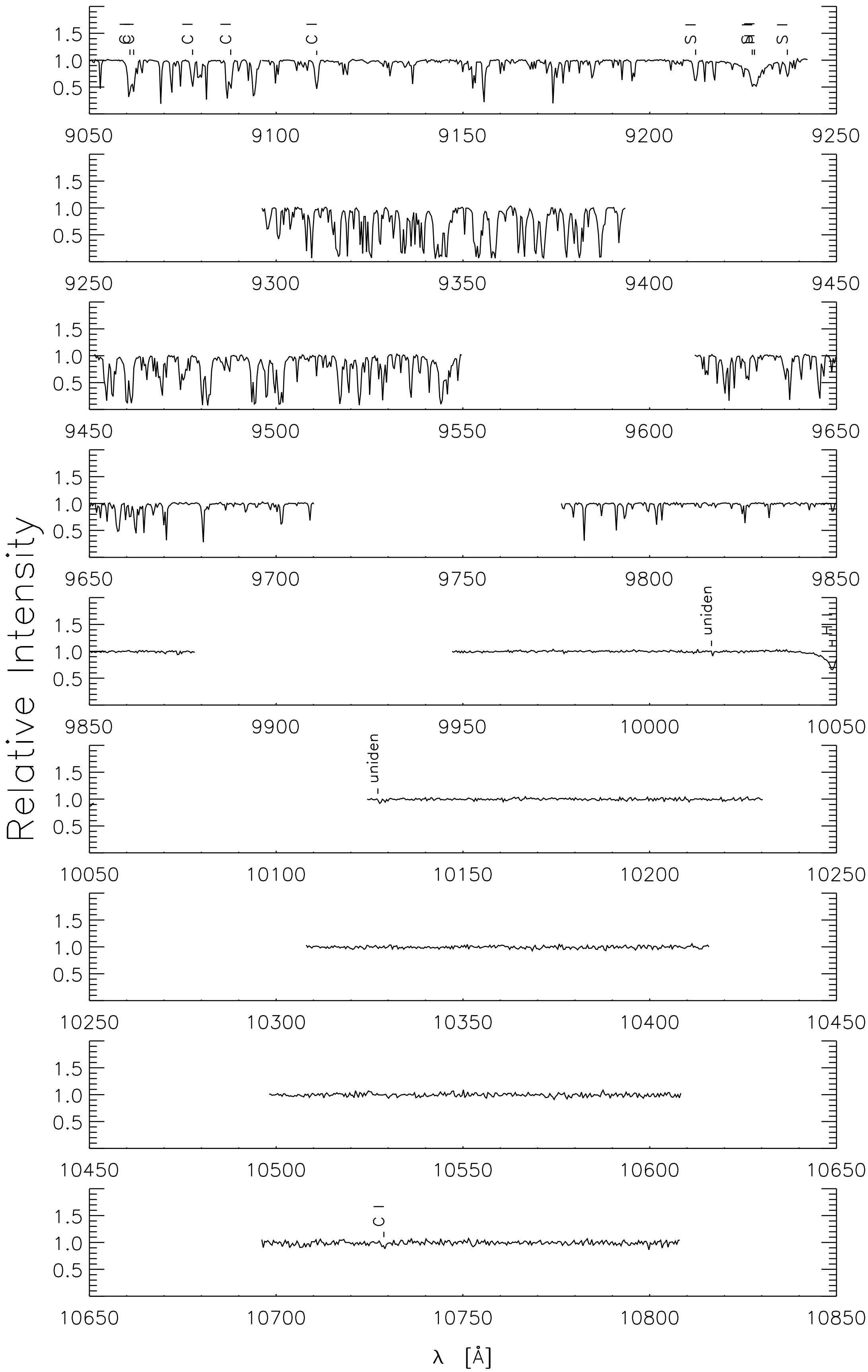

Fig. 9. continued

Table 11. The line identification of HR 4049 from 3650 Å to 10850 Å

$\lambda_{\rm lab}$ [Å]		multiplet	χ [eV]	$\log gf$	$\lambda_{\rm obs}$ [Å]	D [%]	W_λ [mÅ]	$FWHM$ [km/s]	$v_{\rm rad}$ [km/s]	run	Q	remarks
3657.926		H I 7	10.15	-3.189	3657.71	3.3	8	21	-13	3.3	1	H35
3658.641		H I 7	10.15	-3.151	3658.42	4.0	12	23	-14	3.3	1	H34
3659.423		H I 6	10.15	-3.112	3659.16	4.4	14	25	-17	3.3	1	H33
3660.279		H I 6	10.15	-3.072	3660.03	5.2	23	32	-16	3.3	1	H32
3661.221		H I 6	10.15	-3.030	3660.95	7.3	30	34	-18	3.3	1	H31
3662.258		H I 6	10.15	-2.987	3661.96	8.4	47	41	-20	3.3	1	H30
3663.406		H I 6	10.15	-2.942	3663.10	12.1	74	38	-21	3.3	1	H29
3664.679		H I 6	10.15	-2.896	3664.43	14.5	99	44	-16	3.3	1	H28
3666.097		H I 5	10.15	-2.848	3665.81	20.3	125	43	-19	3.3	2	H27
3667.684		H I 5	10.15	-2.799	3667.40	24.9	177	51	-19	3.3	2	H26
3669.466		H I 5	10.15	-2.747	3669.19	29.3	227	54	-18	3.3	2	H25
3671.478		H I 5	10.15	-2.693	3671.20	33.1	266	73	-19	3.3	2	H24
3673.761		H I 5	10.15	-2.637	3673.47	38.5	350	69	-20	3.3	2	H23
3676.365		H I 4	10.15	-2.578	3676.08	42.4	366	78	-19	3.3	2	H22
3679.335		H I 4	10.15	-2.517	3679.07	47.4	542	83	-17	3.3	3	H21
3682.810		H I 4	10.15	-2.452	3682.51	50.6	660	101	-20	3.3	3	H20, a
3686.833		H I 4	10.15	-2.384	3686.57	53.5	811	107	-17	3.3	3	H19, a
3691.557		H I 4	10.15	-2.312	3691.32	58.4	1025	125	-14	3.3	3	H18, a
3697.154		H I 3	10.15	-2.235	3696.83	62.2	1350	138	-22	3.3	2	H17, a
3703.855		H I 3	10.15	-2.154	3703.55	66.6	1639	167	-20	3.3	3	H16, a
3711.973		H I 3	10.15	-2.067	3711.69	67.4	1964	200	-19	3.3	3	H15, a
3721.940		H I 3	10.15	-1.974	3721.67	73.9	2499	236	-17	3.3	2	H14, a
3734.370		H I 2	10.15	-1.873	3734.10	74.1	2824	254	-17	3.3	3	H13, a
3750.154		H I 2	10.15	-1.764	3749.83	78.4	4034	334	-21	3.3	3	H12, a
3757.042		C I 7.04	7.49	-3.550	3756.80	4.5	19	32	-15	3.3	1	b
3770.632		H I 2	10.15	-1.644	3770.35	80.5	5020	361	-18	3.3	1	H11, a, wrong
3797.900		H I 2	10.15	-1.511	3797.61	80.7	4843	347	-19	3.3	3	H10, a
3835.368		H I 2	10.15	-1.362	3835.09	79.4	4060	300	-18	3.3	3	H9, a
3889.051		H I 2	10.15	-1.192	3888.73	79.7	4265	297	-20	3.3	3	H8, a, wrong
3933.664		Ca II 1	0.00	0.150	3933.18	10.0	28	20	-33	3.3	1	A2, CS
3933.664		Ca II 1	0.00	0.150	3933.43	43.8	131	21	-13	3.3	2	B, CS, b
3933.664		Ca II 1	0.00	0.150	3933.71	25.0	44	13	8	3.3	1	C1, IS, b
3933.664		Ca II 1	0.00	0.150	3933.86	32.1	46	10	19	3.3	1	C2, IS, b
3933.664		Ca II 1	0.00	0.150	3933.99	6.0	11	13	30	3.3	1	E1, IS, b
3933.664		Ca II 1	0.00	0.150	3934.18	6.8	10	11	43	3.3	1	E2, IS, b
3933.664		Ca II 1	0.00	0.150	3934.34	3.3	6	13	56	3.3	1	E3, IS, b
3947.295		O I 3	9.15	-2.280	3947.01	5.3	36	49	-17	3.3	1	b
3961.403		C I 17.03	7.68	-2.140	3961.13	4.2	13	23	-17	3.3	1	b
3968.470		Ca II 1	0.00	-0.150	3968.22	13.8	49	25	-14	3.3	1	B, CS, b
3968.470		Ca II 1	0.00	-0.150	3968.64	6.7	15	16	17	3.3	1	C2, IS, b
3968.470		Ca II 1	0.00	-0.150	3969.11	3.4	11	23	53	3.3	1	E3, IS, b
3970.074		H I 2	10.15	-0.993	3969.78	81.6	4800	305	-18	3.3	2	Hϵ
4002.978	*	C I 17.02	7.68	-3.060	4002.55	1.6	4	17	-17	2.3	1	
4009.930		C I 17.01	7.68	-2.780	4009.65	3.9	18	29	-17	3.3	1	
4022.114	*	C I 7.01	7.48	-2.770	4021.67	2.0	8	28	-19	2.3	1	
4022.814	*	C I 7.01	7.48	-2.650	4022.44	2.3	9	28	-14	2.3	1	
	*	unident			4025.68	2.2	14	46		2.3	1	
4029.413		C I 7.01	7.49	-2.190	4029.09	3.2	15	29	-20	3.3	1	
4031.800	*	C I 7.01	7.49	-2.790	4031.36	1.2	5	28	-18	2.3	1	
	*	unident			4032.67	1.9	6	23		4.3	1	
	*	unident			4033.71	1.1	6	39		2.3	1	
4063.577	*	C I 7	7.48	-3.782	4063.50	2.0	11	39	-13	4.3	1	
4064.268		C I 7	7.48	-3.430	4063.94	2.5	7	17	-20	3.3	1	b
4065.243		C I 7	7.49	-3.159	4064.95	3.8	14	25	-17	3.3	1	
4072.643		C I 18.17			4072.35	3.0	15	33	-17	3.3	1	
4101.737		H I 1	10.15	-0.753	4101.39	84.3	5082	272	-21	3.3	3	Hδ
4109.949		N I 10	10.69	-1.200	4109.70	2.0	9	31	-13	3.3	1	b
	*	unident			4150.98	1.7	7	27		2.3	1	
	*	unident			4152.73	1.7	7	27		4.3	1	
	*	unident			4157.23	1.5	6	27		2.3	1	
4212.342		C I 18.12			4212.06	4.6	11	22	-16	3.3	1	
	*	unident			4213.02	1.8	5	18		4.3	1	
4222.466		C I 18.11			4222.16	2.0	6	22	-17	3.3	1	
4223.360		C I 18.11			4222.93	3.3	16	32	-26	3.3	1	b
4228.326		C I 17	7.68	-2.794	4228.01	6.0	25	28	-18	3.3	1	
4269.020		C I 16	7.68	-2.542	4268.68	8.9	31	23	-19	3.3	1	
4340.427		H I 1	10.15	-0.447	4340.06	81.5			-21	3.3	1	Hγ, half profile
4368.242		O I 5	9.52	-2.030	4367.88	6.5	28	29	-21	3.3	1	b
4371.367		C I 14	7.68	-2.333	4371.05	9.5	38	26	-17	3.3	2	
4466.476		C I 18.07			4466.14	2.9	15	32	-18	3.2	1	
4471.477	*	He I 14	20.87	0.050	4471.29	2.5	21	52	-20	4.2	3	
4477.472		C I 18.06			4477.15	4.3	15	22	-17	3.3	1	
4478.588		C I 18.06			4478.27	5.1	32	42	-17	3.2	1	b
4694.113	*	S I 2	6.52	-1.770	4693.60	2.4	8	19	-18	2.2	1	
4734.260	*	C I 18.05	7.95	-2.090	4734.08	2.6	12	26	-19	4.2	1	
4738.461	*	C I 18.05	7.95	-2.360	4738.20	1.7	10	33	-24	4.2	1	b
4762.313		C I 6	7.48	-2.530	4762.03	13.9	87	35	-14	3.2	2	b
4766.672		C I 6	7.48	-2.309	4766.34	5.7	21	22	-17	3.2	1	
4770.027		C I 6	7.48	-2.722	4769.66	7.1	32	27	-18	3.2	2	
4771.742		C I 6	7.49	-2.120	4771.38	19.4	87	26	-18	3.2	3	
4775.897		C I 6	7.49	-2.163	4775.56	9.4	38	24	-17	3.2	2	
4812.920		C I 5	7.48	-3.505	4812.58	1.7	11	37	-17	3.2	1	
4817.373		C I 5	7.48	-3.203	4817.01	3.5	13	22	-18	3.2	1	
4826.796		C I 5	7.49	-2.980	4826.41	1.7	6	22	-19	3.2	1	
4861.279		H I 2	10.15	-0.020	4860.79	82.1	4861	127	-26	3.2	3	Hβ, core
4932.049		C I 13	7.68	-1.844	4931.66	14.9	62	24	-19	3.2	2	
4968.793		O I 14	10.69		4968.42	1.8	7	21	-18	3.2	1	
5017.090	*	C I 18.03	7.95	-0.500	5016.75	1.3	4	28	-6	2.2	1	
5018.068	*	C I 18.03	7.95	-2.000	5017.75	1.3	7	51	-5	2.2	1	
5019.291	*	O I 13	10.74	-1.900	5018.71	1.2	3	16	-20	2.2	1	b
5020.218	*	O I 13	10.74	-1.760	5019.62	0.9	4	24	-21	2.2	1	b
5023.849		C I 18.02	7.95	-2.400	5023.46	2.8	16	31	-19	3.2	1	
5024.916		C I 18.02	7.95	-2.700	5024.63	2.0	7	41	-13	3.2	1	
5039.057		C I 18.01/4	7.95	-2.000	5038.70	6.8	41	34	-17	3.2	1	b
5040.134		C I 18.01	7.95	-2.500	5039.77	2.8	17	29	-17	3.2	1	
5041.660		C I 18.01/4	7.95	-2.500	5041.28	7.8	47	34	-18	3.2	1	b
5052.167		C I 12	7.68	-1.648	5051.78	24.2	115	26	-19	3.2	3	
5153.567	*	C I 26.22	8.65	-4.570	5153.37	1.9	9	26	-19	4.2	1	
5268.948		C I 22.1	8.54	-2.280	5268.52	2.1	10	26	-20	3.2	1	
5329.099		O I 12	10.74	-1.730	5328.70	2.6	12	24	-18	3.2	1	
5329.690		O I 12	10.74	-1.410	5329.29	4.1	16	21	-18	3.2	1	b
5300.550	*	C I 26.19	8.65	-4.190	5300.31	2.1	12	30	-22	4.2	1	b
5330.741		O I 12	10.74	-1.120	5330.34	4.5	24	28	-18	3.2	1	
5380.337		C I 11	7.68	-1.842	5379.94	14.3	77	28	-18	3.1	2	
5545.055		C I 26.14/15	8.64	-2.510	5544.69	4.3	16	26	-15	3.1	1	b

Table 11. continued

$\lambda_{\rm lab}$ [Å]		multiplet	χ [eV]	$\log gf$	$\lambda_{\rm obs}$ [Å]	D [%]	W_λ [mÅ]	$FWHM$ [km/s]	$v_{\rm rad}$ [km/s]	run	Q	remarks
5551.576		C I 26.14	8.64	-2.030	5551.04	1.6	24	27	-25	3.2	1	
5668.943		C I 22.06	8.54	-2.430	5668.54	4.7	21	24	-17	3.1	1	
	*	unident			5706.02	1.7	7	19		4.2	1	
5793.120		C I 18	7.95	-2.157	5792.70	5.0	33	33	-18	3.1	1	
5794.473	*	C I 18	7.95	-2.900	5793.91	1.0	9	43	-15	2.2	1	
5800.594		C I 18	7.95	-2.440	5800.15	2.6	19	23	-19	3.1	1	
5889.953		Na I 1	0.00	0.110	5889.28	24.6	49	10	-30	3.1	3	A2, CS
5889.953		Na I 1	0.00	0.110	5889.62	42.9	98	11	-12	3.1	3	B, CS
5889.953		Na I 1	0.00	0.110	5889.99	38.9	69	8	6	3.1	1	C1, IS
5889.953		Na I 1	0.00	0.110	5890.16	62.8	111	8	15	3.1	1	C2, IS
5889.953		Na I 1	0.00	0.110	5890.38	20.8	39	9	26	3.1	1	D, IS
5889.953		Na I 1	0.00	0.110	5890.68	6.0	10	8	41	3.1	1	E2, IS
5889.953		Na I 1	0.00	0.110	5890.85	6.8	12	8	50	3.1	1	D3, IS
5895.923		Na I 1	0.00	-0.190	5895.26	13.7	27	9	-29	3.1	2	A2, CS
5895.923		Na I 1	0.00	-0.190	5895.61	27.5	58	10	-12	3.1	2	B, CS
5895.923		Na I 1	0.00	-0.190	5895.96	21.5	38	8	6	3.1	1	C1, IS
5895.923		Na I 1	0.00	-0.190	5896.14	48.0	78	8	15	3.1	1	C2, IS
5895.923		Na I 1	0.00	-0.190	5896.37	12.8	23	8	27	3.1	1	D, IS
5895.923		Na I 1	0.00	-0.190	5896.57	5.0	9	8	37	3.1	1	E1, IS
5895.923		Na I 1	0.00	-0.190	5896.83	7.8	14	8	51	3.1	1	E2, IS
6001.121		C I 26.07	8.64	-2.070	6000.67	3.1	5	26	-18	3.1	1	
6002.983	*	C I 26.08	8.65	-2.050	6002.65	1.9	10	25	-24	4.1	1	
6006.021		C I 26.08	8.65	-3.290	6005.56	3.1	16	24	-18	3.2	1	
6007.175		C I 26.07	8.64	-2.180	6006.70	1.8	8	21	-19	3.2	1	
6010.675		C I 26.07	8.64	-2.020	6010.30	2.0	10	23	-14	3.1	1	
6013.166		C I 26.07/06	8.65	-1.370	6012.70	5.6	39	32	-19	3.1	1	b
6014.830		C I 26.07	8.64	-1.710	6014.39	3.6	22	28	-17	3.1	1	
6016.449		C I 26.06	8.64	-1.820	6015.96	1.8	9	25	-20	3.2	1	
		unident			6017.15	2.4	5	10		3.2	1	
6046.233		O I 22	10.99	-1.895	6045.77	1.5	13	42	-18	3.1	1	b
6052.674	*	S I 10	7.87	-0.740	6052.47	2.2	11	24	-18	4.2	1	
6100.445	*	C I 37	8.85	-4.520	6100.25	2.0	12	27	-17	4.2	1	
6155.971		O I 10	10.74	-1.051	6155.53	5.8	36	28	-17	3.1	1	b
6156.778		O I 10	10.74	-0.731	6156.28	7.4	45	28	-20	3.1	1	b
6158.187		O I 10	10.74	-0.441	6157.70	9.8	59	28	-19	3.2	1	
6300.311		[OI] 1F	0.00	-9.819	6299.57	-3.9	-11	13	-31	3.2	1	CS, f
6453.602		O I 9	10.74	-1.364	6453.12	1.2	8	27	-18	3.1	1	b
6454.444		O I 9	10.74	-1.144	6453.96	1.7	11	27	-18	3.1	1	b
6455.977		O I 9	10.74	-0.994	6455.51	1.8	15	37	-17	3.1	1	
6562.817		H I 1	10.15	0.710	6561.31	61.9	2537	103	-64	3.2	3	Hα
6587.610		C I 22	8.54	-1.596	6587.13	10.9	68	27	-18	3.1	1	b
6655.517		C I 21.03	8.54	-1.370	6655.05	1.2	11	41	-17	3.2	1	
	*	unident			6735.37	4.1	14	14		2.1	1	
6743.531		S I 8	7.87	-0.920	6743.12	1.3	8	17	-14	3.2	1	
6748.837		S I 8	7.87	-0.600	6748.26	2.1	26	20	-21	3.2	1	
6757.171		S I 8	7.87	-0.310	6756.69	2.5	19	30	-17	3.1	1	
6828.115		C I 21	8.54	-1.280	6827.64	2.9	24	35	-17	3.2	1	
7093.237		C I 26.01	8.65	-3.260	7092.82	2.0	13	25	-13	3.1	1	
7100.124		C I 25.02	8.64	-1.600	7099.55	3.6	24	27	-20	3.1	1	
7108.934		C I 25.02	8.64	-1.680	7108.40	3.3	18	22	-18	3.1	1	
7111.472		C I 26	8.64	-0.810	7110.95	6.0	44	29	-17	3.1	1	
7113.178		C I 26	8.65	-0.350	7112.63	11.3	72	25	-19	3.1	2	
7115.172		C I 25.02	8.64	-0.710	7114.66	11.3	75	26	-17	3.1	1	b
7116.991		C I 25.02	8.65	-0.910	7116.44	11.6	76	26	-19	3.1	2	
7119.656		C I 25.02	8.64	-1.220	7119.11	8.3	56	27	-18	3.1	1	b
7423.641		N I 3	10.33	-0.760	7423.03	5.1	43	32	-20	3.1	1	
7442.298		N I 3	10.33	-0.454	7441.70	8.9	70	30	-20	3.1	1	
7468.312		N I 3	10.34	-0.270	7467.72	12.8	92	27	-19	3.1	2	
7476.176		C I 29.03	8.77	-0.760	7475.64	1.8	9	18	-17	3.1	1	
7483.445		C I 29.03	8.77	-0.490	7482.96	3.1	22	27	-15	3.1	1	
7771.944		O I 1	9.15	0.324	7771.40	55.6	493	32	-17	3.1	2	
7774.166		O I 1	9.15	0.174	7773.61	53.5	436	30	-17	3.1	3	
7775.388		O I 1	9.15	-0.046	7774.83	47.6	377	29	-17	3.1	3	
	*	unident			7851.38	1.0	6	20		2.1	1	
7852.862	*	C I 32	8.85	-1.420	7852.05	2.5	14	20	-17	2.1	1	
7860.889	*	C I 32	8.85	-0.730	7860.07	3.7	31	30	-17	2.1	1	
		unident			7946.79	2.4	18	27		3.1	1	
8058.621		C I 30.01	8.85	-1.180	8058.00	4.1	32	27	-19	3.1	1	
8184.861		N I 2	10.33	-0.418	8184.26	11.2	66	20	-18	3.1	1	b
8188.012		N I 2	10.33	-0.431	8187.41	10.9	98	31	-18	3.1	1	
8223.128		N I 2	10.33	-0.387	8222.50	11.5	120	36	-18	3.1	1	b
8242.389		N I 2	10.34	-0.381	8241.78	10.1	109	37	-18	3.1	1	b
8345.553		H I 11	12.04		8344.86	17.5	648	96	-20	3.1	1	P23, b
8359.006		H I 11	12.04		8358.22	21.0	759	119	-24	3.1	1	P22, b
8374.478		H I 11	12.04		8373.82	23.4	1079	125	-19	3.1	1	P21, b
8392.400		H I 11	12.04	-1.892	8391.70	28.6	1441	115	-21	3.1	1	P20, b
8413.321		H I 10	12.04	-1.823	8412.69	33.1	1717	126	-18	3.1	1	P19,b
8446.359	*	O I 14	9.52	0.170	8445.41	41.0	325	26	-19	2.1	2	b
8446.758	*	O I 14	9.52	-0.050	8445.91	39.0	309	46	-16	2.1	2	b
8467.256		H I 10	12.04	-1.670	8466.65	34.8			-17	3.1	1	P17, half profile, b
8502.487		H I 10	12.04	-1.586	8501.83	42.4	3029	161	-19	3.1	1	P16, b
8542.089		Ca II 2	1.69		8541.62	6.7	34	17	-12	3.1	1	b
8545.384		H I 10	12.04	-1.495	8544.71	40.2			-19	3.1	1	P15, half profile, b
8594.000		N I 8	10.68	-0.367	8593.46	4.3	26	20	-14	3.1	1	b
8598.394		H I 9	12.04	-1.398	8597.77	39.1			-17	3.1	1	P14, half profile, b
8629.235		N I 8	10.69	0.027	8628.53	17.8	160	29	-20	3.1	2	
8655.878		N I 8	10.69	-0.650	8655.19	5.6	57	33	-20	3.1	1	
8662.140		Ca II 2	1.69	-0.730	8661.68	4.1	26	21	-11	3.1	1	b
8665.021		H I 9	12.04	-1.291	8664.35	43.8	2383	129	-19	3.1	2	P13, b
8680.282		N I 1	10.34	0.236	8679.58	28.7	287	32	-20	3.1	2	b
8683.403		N I 1	10.33	-0.045	8682.73	22.7	215	31	-19	3.1	1	
8728.910		N I 1	10.33	-1.164	8728.19	3.6	40	36	-20	3.1	1	b
8750.475		H I 9	12.04	-1.175	8749.82	46.8	2543	115	-18	3.1	3	P12, b
8862.787		H I 9	12.04	-1.046	8862.19	43.8			-16	3.1	1	P11, half profile, b
		unident			8872.63	4.0	35	28		3.1	1	b
8873.364	*	C I 49	9.00	-1.080	8873.04	4.0	38	31	-19	4.1	1	b
		unident			8873.81	2.1	19	28		3.1	1	b
8874.423	*	S I 21	8.42	-0.050	8874.07	3.0	17	18	-20	4.1	1	b
9014.911		H I 9	12.04	-0.901	9014.28	48.2			-16	3.1	1	P10, half profile, b
9061.436		C I 3	7.48	-0.335	9060.87	58.0	514	28	-14	3.1	1	b
9062.487		C I 3	7.48	-0.432	9061.85	58.0	460	25	-17	3.1	1	b
9078.288		C I 3	7.48	-0.557	9077.64	49.6	437	27	-17	3.1	2	b
9088.513		C I 3	7.48	-0.432	9087.85	53.7	516	30	-17	3.1	1	b
9111.850	*	C I 13	7.49	-0.335	9110.87	54.0	556	30	-18	2.1	3	
9212.910		S I 1	6.50	0.41	9212.31	38.6	506	40	-15	3.1	3	

Table 11. continued

$\lambda_{\rm lab}$ [Å]	multiplet	χ [eV]	$\log gf$	$\lambda_{\rm obs}$ [Å]	D [%]	W_λ [mÅ]	$FWHM$ [km/s]	$v_{\rm rad}$ [km/s]	run	Q	remarks
9228.110	S I 1	6.50	0.26	9227.45					3.1	1	blended by H I 9
9229.020	H I 9	12.04	-0.735	9228.05	49.1			-27	3.1	1	P9, half profile, b
9237.490	S I 1	6.50	0.04	9236.85	28.4	340	35	-16	3.1	3	
	unident			10016.54	9.1	40	12		3.1	2	
10049.400	H I 8	12.04	-0.303	10048.83	34.0			-12	3.1	1	Pδ, half profile, b
	unident			10127.23	3.2	61	53		3.1	1	
10729.530	C I 1	7.48	-0.401	10728.83	10.7	109	27	-15	3.1	1	